

Polynomial fitting and interpolation on circular sections ^{*}

A. Sommariva and M. Vianello ¹

Dept. of Mathematics, University of Padova (Italy)

December 22, 2014

Abstract

We construct Weakly Admissible polynomial Meshes (WAMs) on circular sections, such as symmetric and asymmetric circular sectors, circular segments, zones, lenses and lunes. The construction resorts to recent results on subperiodic trigonometric interpolation. The paper is accompanied by a software package to perform polynomial fitting and interpolation at discrete extremal sets on such regions.

2000 AMS subject classification: 41A10, 41A63, 65D05.

Keywords: Weakly Admissible Meshes (WAMs), discrete extremal sets, polynomial fitting, polynomial interpolation, circular sectors, circular segments, circular zones, circular lenses, circular lunes.

1 Introduction

In the recent literature on multivariate polynomial approximation, the notion of “Weakly Admissible Mesh” has emerged as a basic tool, from both the theoretical and the computational point of view; cf., e.g., [4, 6, 12] and the references therein.

We recall that a Weakly Admissible Mesh (WAM) is a sequence of finite subsets of a multidimensional compact set, say $\mathcal{A}_n \subset K \subset \mathbb{R}^d$ (or \mathbb{C}^d), which are *norming sets* for total-degree polynomial subspaces,

$$\|p\|_K \leq C(\mathcal{A}_n) \|p\|_{\mathcal{A}_n}, \quad \forall p \in \mathbb{P}_n^d(K), \quad (1)$$

where both $C(\mathcal{A}_n)$ and $\text{card}(\mathcal{A}_n)$ increase at most polynomially with n . Here and below, $\mathbb{P}_n^d(K)$ denotes the space of d -variate polynomials of degree

^{*}Supported the ex-60% funds and by the biennial project CPDA124755 of the University of Padova, and by the INdAM GNCS.

¹corresponding author: e-mail: marcov@math.unipd.it

not exceeding n (restricted to K), and $\|f\|_X$ the sup-norm of a function f bounded on the (discrete or continuous) set X . Moreover, we shall term $C(\mathcal{A}_n)$ the “constant” of the WAM. Observe that necessarily $\text{card}(\mathcal{A}_n) \geq \dim(\mathbb{P}_n^d(K))$. When $C(\mathcal{A}_n)$ is bounded we speak of an “Admissible Mesh” (AM), sometimes also called “polynomial mesh” in the literature (cf., e.g., [23, 33, 29, 30]).

Among their properties, we quote that WAMs are preserved by affine transformations, can be constructed incrementally by finite union and product, and are “stable” under small perturbations [28]. Moreover, we recall that unisolvent interpolation point sets, with slowly (at most polynomially) increasing Lebesgue constant, are WAMs, with $C(\mathcal{A}_n)$ equal to the Lebesgue constant and $\text{card}(\mathcal{A}_n) = \dim(\mathbb{P}_n^d(K))$. It has been shown in the seminal paper [12] that WAMs are nearly optimal for polynomial least-squares approximation in the uniform norm, in the sense that

$$\|f - \mathcal{L}_{\mathcal{A}_n} f\|_K \lesssim C(\mathcal{A}_n) \sqrt{\text{card}(\mathcal{A}_n)} \inf_{p \in \mathbb{P}_n^d(K)} \|f - p\|_K, \quad \forall f \in C(K), \quad (2)$$

where $\mathcal{L}_{\mathcal{A}_n}$ denotes the least-squares projection operator.

On the other hand, discrete extremal sets (of Fekete and Leja type) extracted from such meshes show good Lebesgue constants and behave asymptotically as the corresponding continuum extremal sets; we refer the reader, e.g., to [4, 5], and to the excellent survey [3] on the state of the art in multivariate polynomial interpolation and approximation.

In the present paper, we connect the theory of WAMs to the recently developed theory of “*subperiodic*” trigonometric interpolation, that is interpolation by trigonometric polynomials on subintervals of the period. The main motivation for the study of the subperiodic case, came from its connection with polynomial approximation and numerical quadrature on multivariate domains that are related to circular arcs. The case of solids of rotation was considered in [20]. Gaussian subperiodic trigonometric rules and subperiodic transformations were the basis for the construction of algebraic cubature formulas on several circular sections, obtained by linear blending of arcs [8, 15, 16, 14] (such as circular lenses among others), and on circular lunes by suitable subperiodic trigonometric diffeomorphisms [18]. Applications arise, for example, in the framework of optical design, cf. [1].

Here we show how to construct WAMs on arc blending domains and on circular lunes, and we provide the software package [19], written in Matlab, that performs such WAM constructions, as well as polynomial fitting and interpolation at discrete extremal sets on the corresponding domains.

2 WAMs by arc blending

The key tool in all the constructions below is the fact that, by suitable geometric transformations, total-degree bivariate algebraic polynomials on

circular sections belong to tensor-product spaces of trigonometric, or of algebraic with trigonometric, univariate polynomials. In addition to the notations described in the Introduction, we shall denote by $\mathbb{T}_n([\alpha, \beta])$ the $(2n + 1)$ -dimensional subspace of trigonometric polynomials with degree not exceeding n , restricted to the angular interval $[\alpha, \beta]$. Moreover, we shall use the following sets of angular nodes

$$\Xi_k(\alpha, \beta) = \left\{ \theta_j = \psi_j + \frac{\alpha + \beta}{2}, j = 1, 2, \dots, k + 1 \right\} \subset (\alpha, \beta), \quad k > 0, \quad (3)$$

where

$$\psi_j = \psi_j(k, \omega) = 2 \arcsin(\sin(\omega/2)\tau_j) \in (-\omega, \omega), \quad \omega = \frac{\beta - \alpha}{2} \leq \pi,$$

and

$$\tau_j = \tau_{j,k+1} = \cos\left(\frac{(2j-1)\pi}{2(k+1)}\right) \in (-1, 1), \quad j = 1, 2, \dots, k + 1$$

are the zeros of the $(k + 1)$ -th Chebyshev polynomial $T_{k+1}(\tau)$ in $(-1, 1)$. In particular, a key role will be played by

$$\Theta_n = \Theta_n(\alpha, \beta) = \Xi_{2n}(\alpha, \beta). \quad (4)$$

We begin with the following basic inequality for trigonometric polynomials on subintervals of the period.

Lemma 1 *Let be $t \in T_n([\alpha, \beta])$ with $0 < \beta - \alpha \leq 2\pi$, and Θ_n the angular nodal set (4). Then the following inequality holds*

$$\|t\|_{[\alpha, \beta]} \leq C_n \|t\|_{\Theta_n}, \quad C_n = \mathcal{O}(\log n). \quad (5)$$

Proof. In [8], resorting to the nonlinear transformation

$$\theta(\tau) = 2 \arcsin((\sin(\omega/2)\tau)) \in [\omega, \omega], \quad \text{for } \tau \in [-1, 1], \quad (6)$$

with inverse

$$\tau(\theta) = \frac{\sin(\theta/2)}{\sin(\omega/2)} \in [-1, 1], \quad \text{for } \theta \in [-\omega, \omega], \quad (7)$$

it was proved that the $2n + 1$ Chebyshev-like angles $\{\psi_j\}$ in (3) for $k = 2n$ are unisolvent for trigonometric interpolation of degree n in $[-\omega, \omega]$, with cardinal functions expressible in terms of the fundamental Lagrange polynomials of the Chebyshev points $\{\tau_j\}$ in $[-1, 1]$. Moreover, in [17] it was proved that their Lebesgue constant, say C_n , is independent of ω and increases logarithmically with respect to the degree, $C_n = \mathcal{O}(\log n)$. Clearly,

all these properties are shift-invariant and hence are inherited by any angular interval $[\alpha, \beta]$ with $\beta - \alpha \leq 2\pi$.

Now, calling L_n the trigonometric interpolation operator at Θ_n , we have $L_n t \equiv t$ for every $t \in \mathbb{T}_n([\alpha, \beta])$, and thus $\|t\|_{[\alpha, \beta]} = \|L_n t\|_{[\alpha, \beta]} \leq \|L_n\| \|t\|_{\Theta_n} = C_n \|t\|_{\Theta_n}$. \square

Remark 1 Observe that, generalizing the notion, Θ_n in Lemma 1 can be viewed as a WAM for univariate trigonometric polynomials, with logarithmically increasing constant. Moreover, by a slight extension of the arguments in [36] (that we do not report for brevity), it can be proved that $\Xi_{\lceil m\pi n \rceil}(\alpha, \beta)$, $m > 1$, is an Admissible Mesh (AM) for $\mathbb{T}_n([\alpha, \beta])$ with constant $C_n \equiv C = m/(m - 1)$ and cardinality $\lceil m\pi n \rceil + 1$.

The first circular sections that we consider belong to the more general family of domains obtained by *linear blending of elliptical arcs*. This family has been extensively studied in [14], in view of the construction of product Gaussian formulas. Differently from [14], here we do not need that the underlying transformation is injective. Let

$$P(\theta) = A_1 \cos(\theta) + B_1 \sin(\theta) + C_1, \quad Q(\theta) = A_2 \cos(\theta) + B_2 \sin(\theta) + C_2, \quad (8)$$

$\theta \in [\alpha, \beta]$, be two trigonometric planar curves of degree one,

$$A_i = (a_{i1}, a_{i2}), \quad B_i = (b_{i1}, b_{i2}), \quad C_i = (c_{i1}, c_{i2}), \quad i = 1, 2, \quad (9)$$

being suitable bidimensional vectors (with A_i, B_i not all zero), with the important property that the curves are both parametrized on the *same angular interval* $[\alpha, \beta]$, $0 < \beta - \alpha \leq 2\pi$. It is not difficult to show, by a possible riparametrization with a suitable angle shift when A_i and B_i are not orthogonal, that these curves are arcs of two ellipses centered at C_1 and C_2 , respectively (cf. [14]).

Consider the compact domain

$$\Omega = \{(x, y) = \xi(s, \theta) = sP(\theta) + (1 - s)Q(\theta), \quad (s, \theta) \in [0, 1] \times [\alpha, \beta]\}, \quad (10)$$

which is the transformation of the rectangle $[0, 1] \times [\alpha, \beta]$ obtained by convex combination (linear blending) of the arcs $P(\theta)$ and $Q(\theta)$. Observe that the transformation ξ is analytic and not injective, in general.

We can now prove the following

Proposition 1 *Let $X_n = \{s_i\}$ be the set of $n + 1$ Chebyshev-Lobatto points in $[0, 1]$, namely $s_i = \frac{1}{2}(1 + \cos(i\pi/n))$, $i = 0, \dots, n$. Let Θ_n be the set of the $2n + 1$ angular nodes (4).*

The sequence of finite subsets $\mathcal{A}_n = \xi(X_n \times \Theta_n)$ is a WAM of Ω defined in (10), with constant $C(\mathcal{A}_n) = \mathcal{O}(\log^2 n)$.

Proof. Let $p \in \mathbb{P}_n^2(K)$. By the transformation (10) we have that $p(\xi(s, \theta))$ belongs to the tensor-product space $\mathbb{P}_n^1([0, 1]) \otimes \mathbb{T}_n([\alpha, \beta])$. Now, X_n is an algebraic WAM for $[0, 1]$ with constant $\Lambda_n = \mathcal{O}(\log n)$ (being formed by Chebyshev interpolation nodes), whereas Θ_n is a trigonometric WAM for $[\alpha, \beta]$ with constant $C_n = \mathcal{O}(\log n)$ (cf. Lemma 1 and Remark 1).

Then, for every $q \in \mathbb{P}_n^1([0, 1]) \otimes \mathbb{T}_n([\alpha, \beta])$ we can write the chain of inequalities

$$\begin{aligned} \|q\|_{[0,1] \times [\alpha, \beta]} &= |q(s^*, \theta^*)| \leq \Lambda_n \|q(\cdot, \theta^*)\|_{X_n} = \Lambda_n |q(s_{i^*}, \theta^*)| \\ &\leq \Lambda_n C_n \|q(s_{i^*}, \cdot)\|_{\Theta_n} = \Lambda_n C_n |q(s_{i^*}, \theta_{j^*})| \leq \Lambda_n C_n \|q\|_{X_n \times \Theta_n}, \end{aligned}$$

where we have used the fact that $q(\cdot, \theta)$ is an algebraic polynomial for any fixed θ and $q(s, \cdot)$ is a trigonometric polynomial for any fixed s , and (s^*, θ^*) , s_{i^*} and θ_{j^*} are suitable maximum points. It follows that

$$\|p\|_{\Omega} = \|p \circ \xi\|_{[0,1] \times [\alpha, \beta]} \leq \Lambda_n C_n \|p \circ \xi\|_{X_n \times \Theta_n} = \Lambda_n C_n \|p\|_{\xi(X_n \times \Theta_n)}.$$

This shows that $\mathcal{A}_n = \xi(X_n \times \Theta_n)$ is a WAM of Ω defined in (10), with constant $C(\mathcal{A}_n) = \Lambda_n C_n = \mathcal{O}(\log^2 n)$. \square

Notice that $\text{card}(\mathcal{A}_n) \leq (n+1)(2n+1) = 2n^2 + 3n + 1$, since the transformation can be non injective and multiple points can occur. Clearly, other WAMs can be constructed with the same structure and constant growth, for example choosing for X_n the classical Chebyshev points instead of the Chebyshev-Lobatto points, or other optimal families of algebraic interpolation nodes (cf., e.g., [24, Ch. 4]).

2.1 Examples

Several instances of standard as well as less standard sections of disks (and ellipses) can be treated by arc blending, as it has been shown in [14] in the framework of cubature. All the examples below can be reproduced by the Matlab software package WAM in [19]. The software automatically eliminates possible point repetitions when the transformation is not injective.

2.1.1 Symmetric annular sectors

Symmetric annular sectors of a disk with radius R_1 centered in (a, b) , corresponding to an arc with angular interval $[\alpha, \beta]$, are defined by (8)-(10) where $A_1 = (R_1, 0)$, $B_1 = (0, R_1)$, $C_1 = (a, b)$, and $A_2 = (R_2, 0)$, $B_2 = (0, R_2)$, $C_2 = (a, b)$, $0 \leq R_2 < R_1$. A standard circular sector with vertex in the center corresponds to the degenerate case $R_2 = 0$, i.e., $A_2 = (0, 0)$, $B_2 = (0, 0)$ and $Q(\theta) \equiv C_2 = (a, b)$.

The cardinality of the WAM given by Proposition 1 is $2n^2 + 3n + 1$ in the annular case ($R_2 > 0$), whereas it is $2n^2 + 3n + 1 - 2n = 2n^2 + n + 1$ when $R_2 = 0$, since we have to subtract the repetitions of the vertex.

See Figure 1, where $(a, b) = (0, 0)$, $R_1 = 1$, and $R_2 = 0$, $\alpha = \pi/6$, $\beta = \pi/2$ (left), whereas $R_2 = 1/3$, $\alpha = -\pi/3$, $\beta = \pi$ (right).

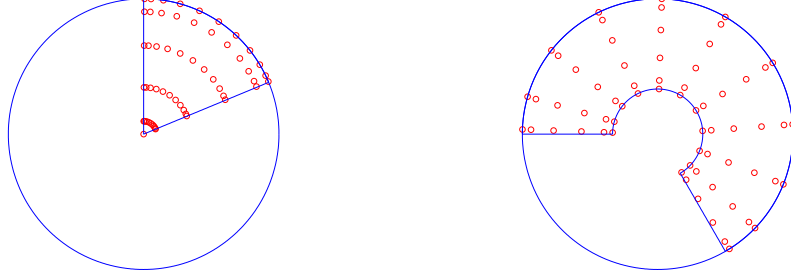


Figure 1: WAMs for degree 5 on a circular sector and an annular sector.

2.1.2 Asymmetric sectors and asymmetric annuli

Asymmetric circular sectors of a disk with radius R centered in (a, b) , corresponding to an arc with angular interval $[\alpha, \beta]$, whose vertex is in any point (c, d) of the disk, are given by (8)-(10) with $A_1 = (R, 0)$, $B_1 = (0, R)$, $C_1 = (a, b)$, and $A_2 = (0, 0)$, $B_2 = (0, 0)$, $C_2 = (c, d)$. Here the WAM cardinality is $2n^2 + n + 1$.

An asymmetric annulus is a disk with a circular hole of radius $R_2 > 0$, whose center (c, d) is different from the disk center (a, b) . It can be described by $A_1 = (R, 0)$, $B_1 = (0, R)$, $C_1 = (a, b)$, and $A_2 = (R_2, 0)$, $B_2 = (0, R_2)$, $C_2 = (c, d)$, with $[\alpha, \beta] = [-\pi, \pi]$. The WAM cardinality is $2n^2 + 3n + 1$.

See Figure 2, where $(a, b) = (0, 0)$, $R = 1$, and $(c, d) = (0.5, -0.5)$, $R_2 = 0$, $\alpha = -\pi/6$, $\beta = \pi/2$ (left), whereas $(c, d) = (0.5, 0.5)$, $R_2 = 0.2$, $\alpha = -\pi$, $\beta = \pi$ (right).

2.1.3 Circular zones and circular segments

A circular zone is the portion of a disk cut by two parallel lines. Up to a rotation, we can consider the case of vertical lines, corresponding to opposite arcs with angular interval $[\alpha, \beta]$, $0 \leq \alpha < \beta \leq \pi$. The transformation is given by (8)-(10) with $A_1 = (R, 0)$, $B_1 = (0, R)$, $C_1 = (a, b)$, and $A_2 = (R, 0)$, $B_2 = (0, -R)$, $C_2 = (a, b)$. The WAM cardinality is $2n^2 + 3n + 1$.

A special case is a circular segment, one of the two portions of the disk cut by a single line. With no loss of generality, up to a rotation we can consider the circular segment corresponding to an angular interval $[-\omega, \omega]$, that by the zone transformation above would correspond to $\alpha = 0$, $\beta = \omega$.

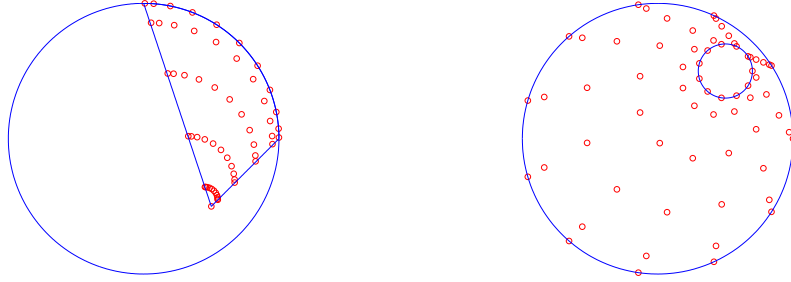


Figure 2: WAMs for degree 5 on an asymmetric sector and an asymmetric annulus.

In order to reduce the cardinality, we can exploit symmetry by the same transformation with a different angular interval, $\alpha = -\omega$, $\beta = \omega$. In such a way, the transformation becomes non injective, each internal node of the WAM is repeated twice whereas the node $(R, 0)$ is repeated n times. Hence, the WAM cardinality is $(2n^2 + 3n + 1 - (n + 1))/2 + 1 = n^2 + n + 1$, that is about half the maximal one.

See Figure 3, where $(a, b) = (0, 0)$, $R = 1$, and $\alpha = \pi/6$, $\beta = \pi/2$ (left), whereas $\alpha = -\pi/3$, $\beta = \pi/3$ (right).

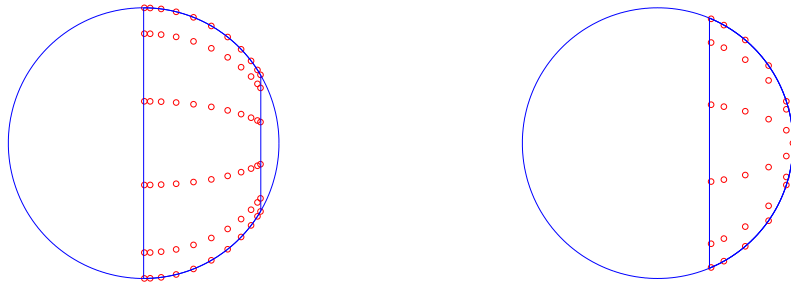


Figure 3: WAMs for degree 5 on a circular zone and a circular segment.

2.1.4 Circular lenses

A circular lens is the intersection of two overlapping disks. When the disks have equal radius, the lens is symmetric. If $\delta = \sqrt{(a - c)^2 + (b - d)^2}$ is the centers distance and R the radius, $\delta < 2R$, the lens is described by (8)-(10) with $A_1 = (R, 0)$, $B_1 = (0, R)$, $C_1 = (a, b)$, and $A_2 = (-R, 0)$, $B_2 = (0, R)$, $C_2 = (c, d)$, and angular interval $\alpha = -\omega$, $\beta = \omega$, $\omega = \arccos(\delta/2)$. The WAM cardinality is $2n^2 + 3n + 1$. See Figure 4-bottom, where $(a, b) = (0, 0)$,

$(c, d) = (0.6, 0)$, $R = 1$.

General lenses, as well as double bubbles (*union* of two overlapping disks), can be treated as union of two circular segments (cf. [18] in the context of cubature). The corresponding WAMs are union of the WAMs of the circular segments, with cardinality $2(n^2 + n + 1)$ and constant which is still $\mathcal{O}(\log^2 n)$, being the maximum of the two constants (cf. [12]). See Figure 4-top.

2.1.5 Butterfly-shaped and candy-shaped regions

A butterfly-shaped region corresponds to linear blending of two opposite circular arcs, that is $A_1 = (R, 0)$, $B_1 = (0, R)$, $A_2 = (-R, 0)$, $B_2 = (0, -R)$, $C_1 = C_2 = (a, b)$, and $\beta - \alpha \leq \pi$. The WAM cardinality is $2n^2 + 3n + 1$ for odd n , and $2n^2 + 2n + 1$ for even n (where we have to subtract the $2n$ repetitions of the centre). See Figure 5-left, where $(a, b) = (0, 0)$, $R = 1$, $\alpha = -\pi/4$, $\beta = \pi/4$.

A candy-shaped region can be generated by linear blending of two symmetric overlapping circular arcs with opposite concavity, that is (up to a rotation) $A_1 = (R, 0)$, $B_1 = (0, R)$, $C_1 = (a, -b)$, and $A_2 = (R, 0)$, $B_2 = (0, -R)$, $C_2 = (a, b)$, $0 < b < R$, $0 < \alpha < \arcsin(b)$, $\beta = \pi - \alpha$. The WAM cardinality is $2n^2 + 3n + 1$ (excluded the exceptional case that at some degree the intersection points of the arcs correspond to Chebyshev-like angular nodes). See Figure 5-right, where $(a, b) = (0, 0.8)$, $R = 1$, $\alpha = \pi/4$, $\beta = 3\pi/4$.

2.1.6 WAMs on the disk by different transformations

The whole disk can be viewed in different ways as linear blending of circular arcs. It can be considered a sector with vertex angle 2π , either symmetric or asymmetric, or a circular zone corresponding to an angular interval of length π . With such transformations, the WAM cardinality is $2n^2 + \mathcal{O}(n)$. See Figure 6.

On the other hand, we can reduce the cardinality by exploiting symmetry. Indeed, we can view the disk as a circular segment with angular interval of length 2π , or as a butterfly-shaped region again with angular interval of length 2π . In such a way the internal nodes are mapped noninjectively in a symmetric way and the resulting cardinality is essentially halved, $n^2 + \mathcal{O}(n)$. See Figure 7.

In Table 1, we summarize the blending parameters for some of the circular sections listed before.

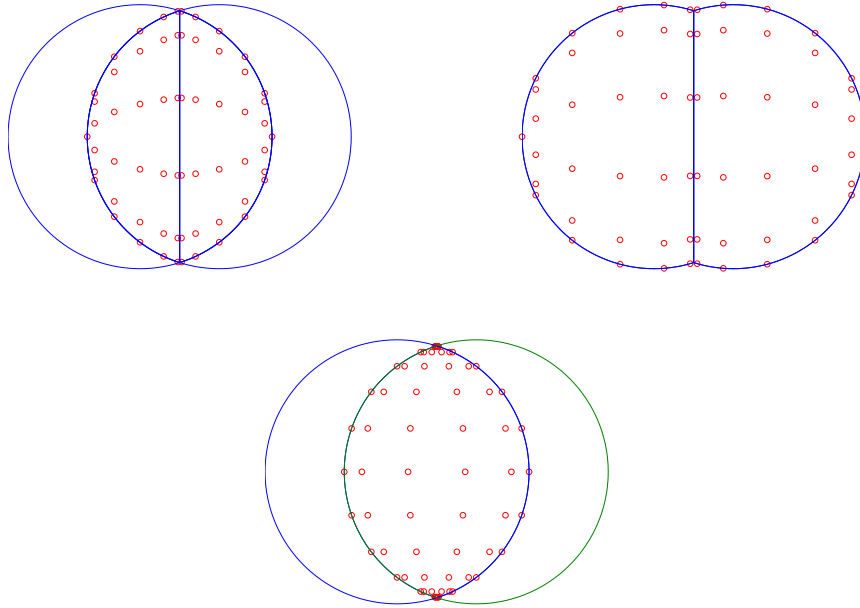


Figure 4: WAMs for degree 5 by union of circular segments on a symmetric lens and a symmetric double bubble (top), and on the same lens by direct transformation (bottom).

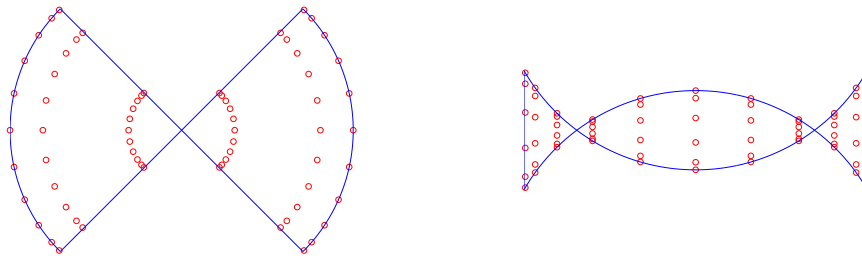


Figure 5: WAMs for degree 5 on a butterfly-shaped (left) and a candy-shaped (right) region.

3 WAMs on lunes

A quite different situation, where only product trigonometric polynomials are involved, is given by circular lunes, that are *difference* of two overlapping disks.

By no loss of generality, up to rotation, translation and scaling, we can consider a lune, say \mathcal{L} , which is the difference of the unit disk with of a disk

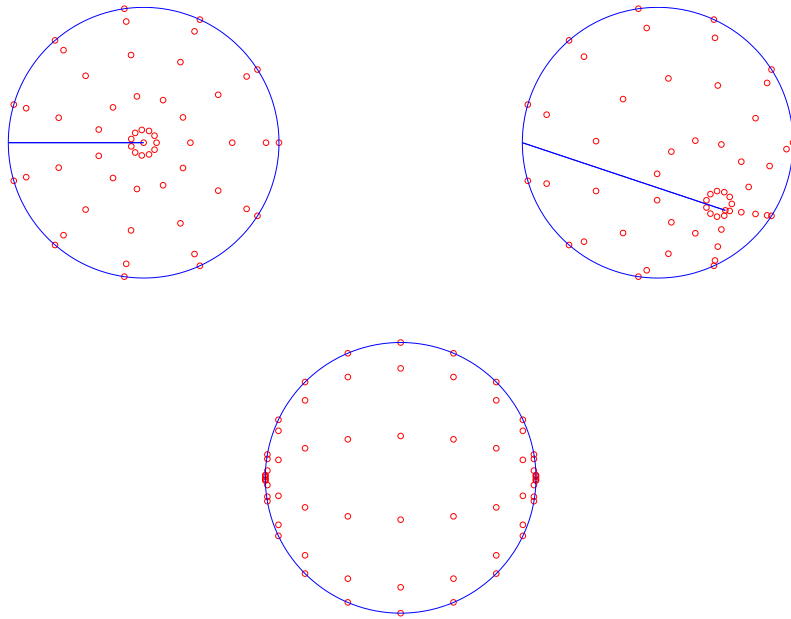


Figure 6: WAMs for degree 5 on the disk, as extremal case of a symmetric sector (top-left), an asymmetric sector (top-right), a circular zone (bottom).

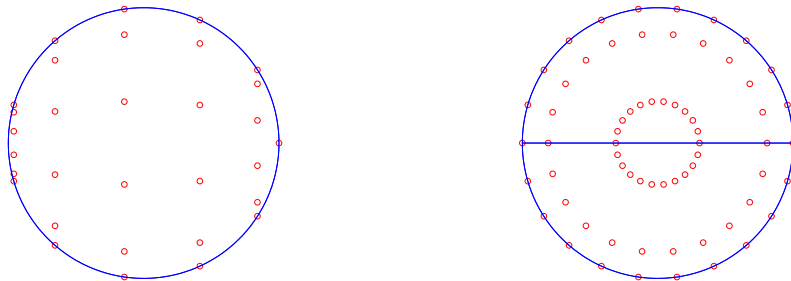


Figure 7: WAMs for degree 5 on the disk as extremal case of a circular segment (left), and a butterfly-shaped region (right).

of radius r centered at $(-d, 0)$, $d > 0$. The condition $|1 - r| < d < 1 + r$ ensures that the intersection is nonempty and one disk is not included into the other, so that we have a proper lune. The boundary of the lune is given by two circular arcs: the right one (longer) is an arc of the unit circle with semiangle ω_2 , the left one (shorter) is an arc of the other circle with

Table 1: Blending parameters in (8)-(10) for some circular sections (for the lens, $\delta < 2R$, $\omega = \arccos(\delta/2)$).

region/parms	A_1	B_1	C_1	A_2	B_2	C_2	ang intv
symm sector	$(R, 0)$	$(0, R)$	(a, b)	$(0, 0)$	$(0, 0)$	(a, b)	$[-\omega, \omega]$
asymm sector	$(R, 0)$	$(0, R)$	(a, b)	$(0, 0)$	$(0, 0)$	(c, d)	$[\alpha, \beta]$
circ zone	$(R, 0)$	$(0, R)$	(a, b)	$(-R, 0)$	$(0, R)$	(a, b)	$[\alpha, \beta]$
circ segment	$(R, 0)$	$(0, R)$	(a, b)	$(R, 0)$	$(0, -R)$	(a, b)	$[-\omega, \omega]$
symm lens	$(R, 0)$	$(0, R)$	(a, b)	$(-R, 0)$	$(0, R)$	$(a + \delta, b)$	$[-\omega, \omega]$
butterfly	$(R, 0)$	$(0, R)$	(a, b)	$(-R, 0)$	$(0, -R)$	(a, b)	$[-\omega, \omega]$

semiangle ω_1 , where

$$0 < \omega_1 = \arccos\left(\frac{r^2 + d^2 - 1}{2dr}\right) < \omega_2 = \arccos\left(\frac{r^2 - d^2 - 1}{2d}\right) < \pi. \quad (11)$$

We consider three bilinear trigonometric transformations of rectangles (in angular variables) to the lune, which have been proposed in [18], of the form

$$\begin{aligned} \sigma(\phi, \theta) = & A_1 + A_2 \cos(\theta) + A_3 \sin(\theta) + A_4 \cos(\phi) + A_5 \cos(\phi) \cos(\theta) \\ & + A_6 \cos(\phi) \sin(\theta) + A_7 \sin(\phi) + A_8 \sin(\phi) \cos(\theta) + A_9 \sin(\phi) \sin(\theta), \end{aligned} \quad (12)$$

where the $A_i = (A_i(1), A_i(2))$ are suitable 2-dimensional vectors, i.e., each component of σ is in the trigonometric space $\mathbb{T}_1 \otimes \mathbb{T}_1$.

The first transformation is

$$\begin{aligned} \sigma_1 = (x(\phi, \theta), y(\phi, \theta)) : & [-\omega_1, \omega_1] \times [0, \omega_2] \rightarrow \mathcal{L}, \quad (13) \\ x(\phi, \theta) = & \cos(\theta) - \frac{\cos(\omega_1)}{\sin(\omega_1)} \sin(\theta) + \frac{1}{\sin(\omega_1)} \cos(\phi) \sin(\theta), \\ y(\phi, \theta) = & \frac{1}{\sin(\omega_1)} \sin(\phi) \sin(\theta). \end{aligned}$$

In [18] it was proved that such a transformation maps (not injectively since $\sigma_1(\phi, 0) \equiv 1$) the boundary of the rectangle onto the boundary of the lune (preserving the orientation) and has positive Jacobian, so that it is a diffeomorphism of the interior of the rectangle onto the interior of the lune.

The second transformation is

$$\begin{aligned} \sigma_2 = (x(\phi, \theta), y(\phi, \theta)) : & [-\omega_1, \omega_1] \times [-\omega_2, \omega_2] \rightarrow \mathcal{L}, \quad (14) \\ x(\phi, \theta) = & \cos(\theta) + \frac{(1 - \cos(\theta)) \sin(\omega_2)}{(1 - \cos(\omega_2)) \sin(\omega_1)} (\cos(\phi) - \cos(\omega_1)), \end{aligned}$$

$$y(\phi, \theta) = \frac{1}{\sin(\omega_1)} \sin(\phi) \sin(\theta) .$$

As proved in [18], under the condition

$$\omega_1 \leq \arctan \left(\frac{2(1 - \cos(\omega_2))}{\sin(\omega_2)} \right) , \quad (15)$$

the transformation maps $[-\omega_1, \omega_1] \times [0, \omega_2]$ onto the lune, diffeomorphically on the interiors, having positive Jacobian. Here we do not need injectivity at all, so in order to reduce the number of nodes we have chosen the rectangle $[-\omega_1, \omega_1] \times [-\omega_2, \omega_2]$, such that now the transformation (14)-(15) is surjective, $\sigma_2(\phi, \theta) = \sigma_2(-\phi, -\theta)$ for every interior point of the rectangle, and $\sigma_2(\phi, 0) \equiv (1, 0)$.

The third transformation is

$$\sigma_3 = (x(\phi, \theta), y(\phi, \theta)) : [-\omega_1, \omega_1] \times [-\omega_2, \omega_2] \rightarrow \mathcal{L} , \quad (16)$$

$$x(\phi, \theta) = (\cos(\phi) - \cos(\omega_1)) \left(\frac{\cos(\omega_2)}{1 - \cos(\omega_1)} + \frac{\sin(\omega_2)}{\sin(\omega_1)} \right) + \frac{1 - \cos(\phi)}{1 - \cos(\omega_1)} \cos(\theta) ,$$

$$y(\phi, \theta) = \frac{1}{\sin(\omega_1)} \sin(\phi) \sin(\theta) .$$

Under the condition

$$(\cos(\omega_2) + \cos(\omega_2 - \omega_1))^2 \leq 4 \cos(\omega_1) , \quad (17)$$

it maps $[0, \omega_1] \times [-\omega_2, \omega_2]$ onto the lune, diffeomorphically on the interiors, having positive Jacobian (cf. [18]). In order to reduce the number of nodes we have chosen again the rectangle $[-\omega_1, \omega_1] \times [-\omega_2, \omega_2]$, such that now the transformation (16)-(17) is surjective, $\sigma_3(\phi, \theta) = \sigma_3(-\phi, -\theta)$ for every interior point of the rectangle, and $\sigma_3(0, \theta) \equiv (-d + r, 0)$.

As discussed in [18], condition (17) determines a set of the parameters ω_1, ω_2 which has nonempty difference with that determined by condition (15). Moreover, when $\omega_1 > \pi/2$, only the general transformation (13) is applicable. The geometric action of the three transformations can be seen in Figure 8.

We are now ready to state and prove the following

Proposition 2 *Let \mathcal{L} the lune defined as the difference of the unit disk with of a disk of radius r centered at $(-d, 0)$, $d > 0$, where $|1 - r| < d < 1 + r$. Let $\Theta_n(\alpha, \beta)$ be the set of the $2n + 1$ angular nodes (4), ω_1, ω_2 the angles defined in (11), σ_i , $i = 1, 2, 3$, the transformations (13), (14)-(15), (16)-(17).*

The sequence of finite subsets $\mathcal{A}_n^{(1)} = \sigma_1(\Theta_n(-\omega_1, \omega_1) \times \Theta_n(0, \omega_2))$ is a WAM of \mathcal{L} , with constant $C(\mathcal{A}_n^{(1)}) = \mathcal{O}(\log^2 n)$ and cardinality $\text{card}(\mathcal{A}_n^{(1)}) = 4n^2 + 4n + 1$. Moreover, for $i = 1, 2$ the sequence of finite subsets $\mathcal{A}_n^{(i)} = \sigma_i(\Theta_n(-\omega_1, \omega_1) \times \Theta_n(-\omega_2, \omega_2))$ is a WAM of \mathcal{L} , with constant $C(\mathcal{A}_n^{(i)}) = \mathcal{O}(\log^2 n)$ and cardinality $\text{card}(\mathcal{A}_n^{(i)}) = 2n^2 + n + 1$.

Proof. Let $p \in \mathbb{P}_n^2(\mathcal{L})$. We have that $p(\sigma_1(\phi, \theta))$ belongs to the tensor-product space $\mathbb{T}_n([-\omega_1, \omega_1]) \otimes \mathbb{T}_n([0, \omega_2])$, whereas $p(\sigma_i(\phi, \theta))$, $i = 1, 2$, belongs to the tensor-product space $\mathbb{T}_n([-\omega_1, \omega_1]) \otimes \mathbb{T}_n([-\omega_2, \omega_2])$. Then, reasoning as in the proof of Proposition 1 we get

$$\|p\|_{\mathcal{L}} = \|p \circ \sigma_1\|_{[-\omega_1, \omega_1] \times [0, \omega_2]} \leq C_n^2 \|p \circ \sigma_1\|_{\Theta_n(-\omega_1, \omega_1) \times \Theta_n(0, \omega_2)} = \|p\|_{\mathcal{A}_n^{(1)}},$$

where $C_n = \mathcal{O}(\log n)$ by Lemma 1. By injectivity of the transformation σ_1 in the interior of the rectangle, the cardinality is $(2n + 1)^2 = 4n^2 + 4n + 1$. The argument is the same for σ_2 and σ_3 , whereas the structure of the transformations entails that the cardinality is essentially halved. In fact, by symmetry of the nodes and of the transformations we have to subtract the node repetitions, so that the cardinality is $((2n + 1)^2 - (2n + 1))/2 + 1 = 2n^2 + n + 1$. \square

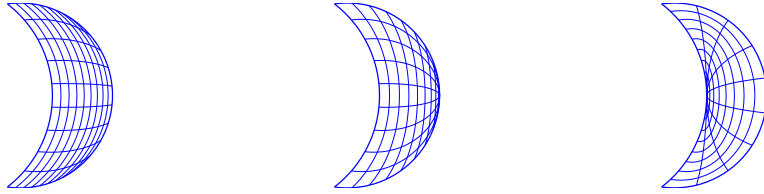


Figure 8: Mapping a 10×10 angular grid from the relevant rectangles to a lune by the three transformations σ_1 , σ_2 , σ_3 .

In Figure 9 we show examples of WAMs on circular lunes, obtained by the transformations σ_1 , σ_2 , σ_3 . The top-left lune is the difference of the disk of radius $r = 0.8$ centered in $(-0.7, 0)$ with the unit disk, with the top-right lune the disks are interchanged, whereas the bottom lune is the difference of the disk of radius $r = 0.8$ centered in $(-0.4, 0)$ with the unit disk.

Remark 2 It is worth observing that in view of Remark 1 and of a well-known univariate polynomial inequality by Ehlich and Zeller [21] (see also [9, Rem. 1]), we can even easily construct an Admissible Mesh on arc-blending domains and on circular lunes. Indeed, reasoning as in the proof of Proposition 1, it turns out that $\xi(X_{mn} \times \Xi_{\lceil m\pi n \rceil}(\alpha, \beta))$, $m > 1$, is an Admissible Mesh for Ω defined in (10), with constant

$$C = \frac{m}{(m-1) \cos\left(\frac{\pi}{2m}\right)}$$

and cardinality not exceeding $(mn + 1)(\lceil m\pi n \rceil + 1) \sim \pi(mn)^2$.

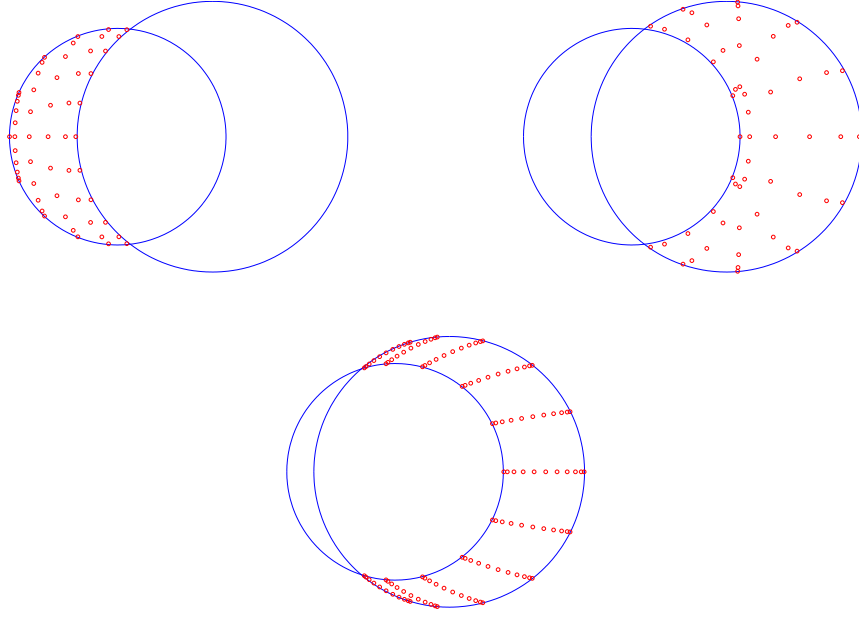


Figure 9: WAMs for degree 5 on three circular lunes, by the transformation σ_1 (bottom), σ_2 (top-left) and σ_3 (top-right).

Similarly, $\sigma_i(\Xi_{\lceil m\pi n \rceil}(-\omega_1, \omega_1) \times \Xi_{\lceil m\pi n \rceil}(-\omega_2, \omega_2))$, $m > 1$, $i = 1, 2, 3$, is an Admissible Mesh for a lune \mathcal{L} , with constant

$$C = \left(\frac{m}{m-1} \right)^2$$

and cardinality $(\pi mn)^2 + \mathcal{O}(n)$ for σ_1 , and $(\pi mn)^2/2 + \mathcal{O}(n)$ for σ_2 and σ_3 .

Working with Admissible Meshes, however, is not really convenient from the computational point of view. For example, taking $m = 2$ we get $C(\mathcal{A}_n) \equiv C = 2\sqrt{2}$ (arc-blending domains) or $C(\mathcal{A}_n) \equiv C = 4$ (lunes), instead of the very slowly increasing $C(\mathcal{A}_n) = \mathcal{O}(\log^2 n)$ of a WAM, but the cardinality is from approximately 6 (arc-blending domains) to approximately 10 (lunes) times higher.

4 Polynomial fitting and polynomial interpolation

The theoretical and computational role of WAMs in multivariate polynomial approximation has been extensively studied in the last years, starting from the seminal paper [12]. We recall here some basic results and algorithms concerning polynomial fitting on WAMs, and polynomial interpolation at discrete extremal sets extracted from WAMs.

Let us term $\mathcal{L}_{\mathcal{A}_n}$ the projection operator $C(K) \rightarrow \mathbb{P}_n^d(K)$ defined by polynomial least-squares on a WAM, and $\mathcal{L}_{\mathcal{F}_n}$ the projection operator defined by interpolation on *Fekete points* of degree n , say \mathcal{F}_n , extracted from a WAM (Fekete points are points that maximize the absolute value of the Vandermonde determinant). Concerning their operator norms with respect to $\|\cdot\|_K$, in [12] it is proved that

$$\|\mathcal{L}_{\mathcal{A}_n}\| \lesssim C(\mathcal{A}_n) \sqrt{\text{card}(\mathcal{A}_n)}, \quad (18)$$

for polynomial least-squares, and

$$\|\mathcal{L}_{\mathcal{F}_n}\| \leq NC(\mathcal{A}_n), \quad N = \dim(\mathbb{P}_n^d(K)), \quad (19)$$

for polynomial interpolation, which show that WAMs with slowly increasing constants $C(\mathcal{A}_n)$ and cardinalities, are relevant structures for multivariate polynomial approximation. The WAMs of *circular sections* studied in the previous sections are good candidates for polynomial fitting and interpolation on the corresponding 2-dimensional regions, since

$$C(\mathcal{A}_n) = \mathcal{O}(\log^2 n), \quad \text{card}(\mathcal{A}_n) = \mathcal{O}(n^2). \quad (20)$$

Moreover, (18)-(19) turn out to be in practice large overestimates of the actual growth.

A standard calculation for projection operators provides from (18)-(19) estimate (2), as well as

$$\|f - \mathcal{L}_{\mathcal{F}_n} f\|_K \lesssim NC(\mathcal{A}_n) \inf_{p \in \mathbb{P}_n^d(K)} \|f - p\|_K, \quad \forall f \in C(K), \quad (21)$$

from which we get, if K is a *Jackson compact* and for a sufficiently regular function f ,

$$\|f - \mathcal{L}_{\mathcal{A}_n} f\|_K = \mathcal{O}\left(C(\mathcal{A}_n) \sqrt{\text{card}(\mathcal{A}_n)} n^{-k}\right), \quad (22)$$

and

$$\|f - \mathcal{L}_{\mathcal{F}_n} f\|_K = \mathcal{O}\left(NC(\mathcal{A}_n) n^{-k}\right), \quad (23)$$

which shows that the least-squares approximation process is theoretically convergent in the uniform norm whenever $k > 1$, and the interpolation process is theoretically convergent whenever $k > 2$ (since $N \sim n^2/2$).

We recall that a *fat compact set* $K \subset \mathbb{R}^d$ (i.e., $K = \overline{K^\circ}$) is termed a Jackson compact if it admits a *Jackson inequality*, namely for each $k \in \mathbb{N}$ there exist a positive integer m_k and a positive constant c_k such that

$$n^k \inf_{p \in \mathbb{P}_n^d(K)} \|f - p\|_K \leq c_k \sum_{|\mathbf{i}| \leq m_k} \|D^{\mathbf{i}} f\|_K, \quad n > k, \quad \forall f \in C^{m_k}(K). \quad (24)$$

Examples of Jackson compacts are d -dimensional cubes (with $m_k = k + 1$) and Euclidean balls (with $m_k = k$).

In [32], it is proved that if a fat compact set K is Whitney-regular and admits a Markov polynomial inequality, then it is a Jackson compact. Now, two deep results based on *subanalytic geometry* and *pluripotential theory* allow to conclude that arc-blending domains and lunes are Jackson compacts. In fact, being an analytic image of a rectangle, they are subanalytic compact subset of \mathbb{R}^2 and then they admit a Markov polynomial inequality; see [27, 32] and the survey [31] for the relevant definitions and proofs. Moreover, being subanalytic they are also Whitney-regular (cf. [35]), a fact that can be proved also directly by geometrical considerations as in [18].

4.1 Computational issues and numerical tests

Below, we describe the computational issues of polynomial approximation on the circular sections of Section 2 and 3. We recall briefly the main features of the approximation procedures, that resort to basic Numerical Linear Algebra methods, referring the reader, e.g., to [4, 5, 7, 34] for a more extensive and deep analysis. All the algorithms are implemented in the Matlab package [19].

The approximation algorithms start from Vandermonde-like matrices in suitable total-degree polynomial bases. The choice of the standard monomial basis is unappropriate already at small degrees, due to its severe ill-conditioning. A general and more suitable choice is the product Chebyshev basis of the smallest Cartesian rectangle (say $[a, b] \times [c, d]$) containing the region, namely

$$T_h \left(\frac{2x - b - a}{b - a} \right) T_k \left(\frac{2y - d - c}{d - c} \right), \quad 0 \leq h + k \leq n.$$

By a suitable ordering (for example the lexicographical ordering), we obtain a polynomial basis that we call

$$\mathbf{p}(x, y) = (p_1(x, y), \dots, p_N(x, y)), \quad N = \dim(\mathbb{P}_n^2) = \frac{(n+1)(n+2)}{2}, \quad (25)$$

and we can compute the corresponding Vandermonde-like matrix on a WAM of the region

$$V(\mathcal{A}_n, \mathbf{p}) = (p_j(x_i, y_i)), \quad 1 \leq i \leq M, \quad 1 \leq j \leq N, \quad (26)$$

where $\mathcal{A}_n = \{(x_1, y_1), \dots, (x_M, y_M)\}$. Notice that $M \geq N$ and $V(\mathcal{A}_n, \mathbf{p})$ is full-rank by (1), cf. [12].

The core of the fitting and interpolation procedures is a two-step discrete orthogonalization of the polynomial basis by the QR algorithm, namely

$$V(\mathcal{A}_n, \mathbf{p}) = Q_1 R_1, \quad Q_1 = Q R_2, \quad (27)$$

where

$$Q = V(\mathcal{A}_n, \boldsymbol{\varphi}) = V(\mathcal{A}_n, \mathbf{p})R_1^{-1}R_2^{-1} \quad (28)$$

is the (numerically) orthogonal Vandermonde-like matrix corresponding to the discrete orthonormal polynomial basis

$$\boldsymbol{\varphi} = (\varphi_1, \dots, \varphi_N) = (p_1, \dots, p_N)R_1^{-1}R_2^{-1}. \quad (29)$$

The reason for iterating the QR factorization is to cope with the strong ill-conditioning which is typical of Vandermonde-like matrices and increases with the degree. Two orthogonalization iterations generally suffice, unless the original matrix $V(\mathcal{A}_n, \mathbf{p})$ is so severely ill-conditioned (rule of thumb: condition number greater than the reciprocal of machine precision) that the algorithm fails (cf. [34]). This phenomenon of “twice is enough”, is well-known in numerical Gram-Schmidt orthogonalization, cf. [22]. In practice, the change of polynomial basis is conveniently implemented by the Matlab matrix right division operator (cf. [25]) as $\boldsymbol{\varphi} = (\mathbf{p}/R_1)/R_2$, in view of the ill-conditioning inherited by the triangular matrices R_1 and R_2 .

The least-squares polynomial projection of $f \in C(K)$, computed on an array of target points $X = \{(\xi_1, \eta_1), \dots, (\xi_S, \eta_S)\} \subset K$, is simply

$$\mathcal{L}_{\mathcal{A}_n} f(X) = V(X, \boldsymbol{\varphi})Q^t \mathbf{f}, \quad \mathbf{f} = (f(\xi_1, \eta_1), \dots, f(\xi_S, \eta_S))^t. \quad (30)$$

Moreover, we can estimate the norm of the least-squares projection operator, that we call its “Lebesgue constant” by analogy with interpolation, by an array of control points Y as

$$\|\mathcal{L}_{\mathcal{A}_n}\| \approx \|Q(V(Y, \boldsymbol{\varphi}))^t\|_1, \quad (31)$$

cf. [6]. In [19], the estimate is repeated with $Y = \mathcal{A}_{kn}$, $k = 2, 3, \dots$, until the ratio of two successive estimates stabilizes around 1. Though the underlying “Lebesgue function” is not a polynomial and thus the use of WAMs as control sets has not a sound theoretical basis, this procedure, adopted for example in [10], turns out to give a good final estimate of the Lebesgue constant.

Concerning polynomial interpolation on circular sections, we resort to the approximate versions of Fekete points of K (points that maximize the absolute value of the Vandermonde determinant) studied in several papers [4, 5, 34]. By (19), it makes sense to start from a WAM, that is from the corresponding orthogonal Vandermonde-like matrix $Q = V(\mathcal{A}_n, \boldsymbol{\varphi})$ in (28) (which is preferable for conditioning issues). The problem of selecting a $N \times N$ square submatrix with maximal determinant from a given $M \times N$ rectangular matrix is known to be NP-hard [13], but can be solved in an approximate way by two simple *greedy* algorithms, that are fully described and analyzed in [5]. These algorithms produce two interpolation nodal sets, called *discrete extremal sets*.

The first, that computes the so-called *Approximate Fekete Points* (AFP), tries to maximize iteratively submatrix volumes until a maximal volume $N \times N$ submatrix of Q is obtained, and can be based on the famous *QR factorization with column pivoting* [11], applied to Q^t (that in Matlab is implemented by the matrix left division or backslash operator, cf. [25]). See [13] for the notion of volume generated by a set of vectors, which generalizes the geometric concept related to parallelograms and parallelepipeds (the volume and determinant notions coincide on a square matrix).

The second, that computes the so-called *Discrete Leja Points* (DLP), tries to maximize iteratively submatrix determinants, and is based simply on *Gaussian elimination with row pivoting* applied to Q .

Denoting by A the $M \times 2$ matrix of the WAM nodal coordinates, the corresponding computational steps, written in a Matlab-like style, are

$$\mathbf{w} = Q \setminus \mathbf{v}; \mathbf{i} = \text{find}(\mathbf{w} \neq \mathbf{0}); \mathcal{F}_n^{AFP} = A(\mathbf{i}, :); \quad (32)$$

for AFP, where \mathbf{v} is any nonzero N -dimensional vector, and

$$[L, U, \boldsymbol{\sigma}] = \text{LU}(Q, \text{"vector"}); \mathbf{i} = \boldsymbol{\sigma}(1 : N); \mathcal{F}_n^{DLP} = A(\mathbf{i}, :); \quad (33)$$

for DLP. In (33), we refer to the Matlab version of the LU factorization that produces a row permutation vector. In both algorithms, we eventually select an index subset $\mathbf{i} = (i_1, \dots, i_N)$, that extracts a Fekete-like discrete extremal set \mathcal{F}_n of the region K from the WAM \mathcal{A}_n . Once one of the discrete extremal sets has been computed, we can simply apply (26)-(31) with the $N \times N$ matrix $V(\mathcal{F}_n, \mathbf{p})$ substituting the $M \times N$ matrix $V(\mathcal{A}_n, \mathbf{p})$, in order to compute the interpolation polynomial $\mathcal{L}_{\mathcal{F}_n}$ and to estimate the Lebesgue constant $\|\mathcal{L}_{\mathcal{F}_n}\|$. This is the procedure implemented in [19].

Remark 3 Once the underlying extraction WAM has been fixed, differently from the continuum Fekete points, Approximate Fekete Points depend on the choice of the basis, and Discrete Leja Points depend also on its order. An important feature is that Discrete Leja Points form a *sequence*, i.e., if the polynomial basis \mathbf{p} is such that its first $N_s = \dim(\mathbb{P}_s^d(K))$ elements span $\mathbb{P}_s^d(K)$, $1 \leq s \leq n$, then the first N_s Discrete Leja Points are a unisolvent set for interpolation in $\mathbb{P}_s^d(K)$.

Under the latter assumption for Discrete Leja Points, the two families of discrete extremal sets share the same asymptotic behavior, which by a recent deep result in pluripotential theory, cf. [2], is exactly that of the continuum Fekete points: the corresponding uniform discrete probability measures converge weakly to the pluripotential theoretic equilibrium measure of the underlying compact set, cf. [3, 4, 5].

We can now give some numerical examples. All the numerical tests have been made in Matlab 7.7.0 with an Athlon 64 X2 Dual Core 4400+ 2.40GHz processor.

First, we compute the Lebesgue constants of discrete least-squares on WAMs and interpolation at discrete extremal sets, on the circular sections listed in Table 1, for $\omega = \pi/3$; observe that the polynomial inequality defining a WAM and the Lebesgue constants are both invariant by affine transformation of a region, so here they are independent of R and (a, b) . The results are collected in Table 2. The family of arc-blending domains, in particular of circular sections, was studied also in [26].

Notice that the least-squares Lebesgue constants are much smaller than the interpolation Lebesgue constants, that the DLP constants tend to be greater than the AFP constants and are prone to large oscillations (see also Figure 10). As already observed, it is theoretically known that the Lebesgue constant of univariate trigonometric interpolation at the Chebyshev-like angles (11) is independent of ω [17]. This implies that also the bounds (18)-(19) are independent of ω .

On the other hand, the actual Lebesgue constants are much smaller than the bounds, but in our numerical experiments with varying ω (not reported for brevity), only the size of the least-squares Lebesgue constants has shown small variations with respect to the arclength, as well as small or moderate variations changing the region. This can be seen, for example, in Table 3, where we display the Lebesgue constants for a circular sector with $\omega = \pi/6, \pi/2, 2\pi/3$, to be compared also with Table 2 where $\omega = \pi/3$.

It is also interesting to compare the Lebesgue constants on the whole disk, treated by the transformations of Section 2.1.6. The numerical results are listed in Table 4.

Concerning lunes, the results are similar to those obtained with arc-blending domains. In Figure 10-right, we have plotted the Lebesgue constants corresponding to the lune of Figure 9 top-right. For the purpose of illustration, in Figures 11 and 12 we show the WAMs and the extracted AFP and DLP points at degree 10 for the lune, and for a circular lens with $\omega = \pi/3$.

Finally, in Figures 13 and 14 we compare the reconstruction error (measured as relative ℓ^2 error on a suitable control mesh) by polynomial least-squares on a WAM and by interpolation at discrete extremal sets, on the lens and the lune of Figures 11-12, by five test functions with different regularity or variation rate: a polynomial, two Gaussians and two fractional power functions centered at an internal point,

$$\begin{aligned} f_1(x, y) &= (x + y + 2)^{10}, \quad f_2(x, y) = \exp(-c[(x - \xi)^2 + (y - \eta)^2]), \\ f_3(x, y) &= ((x - \xi)^2 + (y - \eta)^2)^\delta, \end{aligned} \tag{34}$$

with $c = 1$ and $c = 5$, $\delta = 3/2$ and $\delta = 5/2$. We have that f_2 is an analytic function, whereas $f_3 \in C^2$ for $\delta = 3/2$ with singular third derivatives, and $f_3 \in C^4$ for $\delta = 5/2$ with singular fifth derivatives. Observing Figures 13 and 14, one can notice that the three approximation techniques give closer

errors than what could be predicted from the large differences between the Lebesgue constants.

References

- [1] B. Bauman and H. Xiao, Gaussian quadrature for optical design with noncircular pupils and fields, and broad wavelength range, *Proc. SPIE*, 7652(2) (2010), 1–12.
- [2] R. Berman, S. Boucksom and D. Witt Nyström, Fekete points and convergence towards equilibrium measures on complex manifolds, *Acta Math.* 207 (2011), 1–27.
- [3] T. Bloom, L. Bos, J.-P. Calvi and N. Levenberg, Polynomial interpolation and approximation in \mathbb{C}^d , *Ann. Polon. Math.* 106 (2012), 53–81.
- [4] L. Bos, J.-P. Calvi, N. Levenberg, A. Sommariva and M. Vianello, Geometric Weakly Admissible Meshes, *Discrete Least Squares Approximation and Approximate Fekete Points*, *Math. Comp.* 80 (2011), 1601–1621.
- [5] L. Bos, S. De Marchi, A. Sommariva and M. Vianello, Computing multivariate Fekete and Leja points by numerical linear algebra, *SIAM J. Numer. Anal.* 48 (2010), 1984–1999.
- [6] L. Bos, S. De Marchi, A. Sommariva and M. Vianello, Weakly Admissible Meshes and Discrete Extremal Sets, *Numer. Math. Theory Methods Appl.* 4 (2011), 1–12.
- [7] L. Bos, A. Sommariva and M. Vianello, Least-squares polynomial approximation on weakly admissible meshes: disk and triangle, *J. Comput. Appl. Math.* 235 (2010), 660–668.
- [8] L. Bos and M. Vianello, Subperiodic trigonometric interpolation and quadrature, *Appl. Math. Comput.* 218 (2012), 10630–10638.
- [9] L. Bos and M. Vianello, Low cardinality admissible meshes on quadrangles, triangles and disks, *Math. Inequal. Appl.* 15 (2012), 229–235.
- [10] M. Briani, A. Sommariva and M. Vianello, Computing Fekete and Lebesgue points: simplex, square, disk, *J. Comput. Appl. Math.* 236 (2012), 2477–2486.
- [11] P.A. Businger and G.H. Golub, Linear least-squares solutions by Householder transformations, *Numer. Math.* 7 (1965), 269–276.
- [12] J.P. Calvi and N. Levenberg, Uniform approximation by discrete least squares polynomials, *J. Approx. Theory* 152 (2008), 82–100.

- [13] A. Civril and M. Magdon-Ismaïl, On Selecting a Maximum Volume Sub-matrix of a Matrix and Related Problems, *Theoretical Computer Science* 410 (2009), 4801–4811.
- [14] G. Da Fies, A. Sommariva and M. Vianello, Algebraic cubature by linear blending of elliptical arcs, *Appl. Numer. Math.* 74 (2013), 49–61.
- [15] G. Da Fies and M. Vianello, Trigonometric Gaussian quadrature on subintervals of the period, *Electron. Trans. Numer. Anal.* 39 (2012), 102–112.
- [16] G. Da Fies and M. Vianello, Algebraic cubature on planar lenses and bubbles, *Dolomites Res. Notes Approx. DRNA* 5 (2012), 7–12.
- [17] G. Da Fies and M. Vianello, On the Lebesgue constant of subperiodic trigonometric interpolation, *J. Approx. Theory* 167 (2013), 59–64.
- [18] G. Da Fies and M. Vianello, Product Gaussian quadrature on circular lunes, *Numer. Math. Theory Methods Appl.* 7 (2014), 251–264.
- [19] S. De Marchi, F. Piazzon, A. Sommariva and M. Vianello, WAM: Matlab package for polynomial fitting and interpolation on Weakly Admissible Meshes, available online at <http://www.math.unipd.it/~marcov/CAAssoft>.
- [20] S. De Marchi and M. Vianello, Polynomial approximation on pyramids, cones and solids of rotation, *Dolomites Res. Notes Approx. DRNA* 6 (2013), 20–26.
- [21] H. Ehlich and K. Zeller, Schwankung von Polynomen zwischen Gitterpunkten, *Math. Z.*, **86**, (1964), 41–44.
- [22] L. Giraud, J. Langou, M. Rozložnik and J. van den Eshof, Rounding error analysis of the classical Gram-Schmidt orthogonalization process, *Numer. Math.* 101 (2005), 87–100.
- [23] A. Kroó, On optimal polynomial meshes, *J. Approx. Theory* 163 (2011), 1107–1124.
- [24] G. Mastroianni and G.V. Milovanović, *Interpolation Processes: Basic Theory and Applications*, Springer Monographs in Mathematics, Springer-Verlag, Berlin, 2008.
- [25] Mathworks, Matlab documentation (2014), available online at: <http://www.mathworks.com/help/matlab>.
- [26] A. Passarini, Computation of discrete extremal sets on circular sections, Laurea Thesis in Mathematics (in Italian), University of Padova, 2013 (advisor: M. Vianello).

- [27] W. Pawłucki and W. Pleśniak, Markov's Inequality and C^∞ Functions on Sets with Polynomial Cusps, *Math. Ann.* 275 (1986), 467–480.
- [28] F. Piazzon and M. Vianello, Small perturbations of polynomial meshes, *Appl. Anal.* 92 (2013), 1063–1073.
- [29] F. Piazzon and M. Vianello, Sub-optimal polynomial meshes on planar Lipschitz domains, *Numer. Funct. Anal. Optim.* 35 (2014), 1467–1475.
- [30] F. Piazzon and M. Vianello, Constructing optimal polynomial meshes on planar starlike domains, *Dolomites Res. Notes Approx. DRNA* 7 (2014), 22–25.
- [31] W. Pleśniak, Multivariate polynomial inequalities via pluripotential theory and subanalytic geometry methods, *Banach Center Publ.* 72 (2006), 251–261.
- [32] W. Pleśniak, Multivariate Jackson Inequality, *J. Comput. Appl. Math.* 233 (2009), 815–820.
- [33] W. Pleśniak, Nearly optimal meshes in subanalytic sets, *Numer. Algorithms* 60 (2012), 545–553.
- [34] A. Sommariva and M. Vianello, Computing approximate Fekete points by QR factorizations of Vandermonde matrices, *Comput. Math. Appl.* 57 (2009), 1324–1336.
- [35] J. Stasica, The Whitney condition for subanalytic sets, *Zeszyty Nauk. Uniw. Jagiellon. Prace Mat.* 23 (1982), 211–221.
- [36] M. Vianello, Norming meshes by Bernstein-like inequalities, *Math. Inequal. Appl.* 17 (2014), 929–936.

Table 2: Lebesgue constants of least-squares and interpolation at discrete extremal sets on the circular sections of Table 1 for $\omega = \pi/3$.

region/degree		3	6	9	12	15	18	21	24
symm sector	LS	2.6	3.5	4.3	5.1	5.7	6.3	6.8	7.3
	AFP	3.9	7.4	13.8	20.5	33.7	40.5	52.6	74.3
	DLP	5.2	9.8	15.6	30.1	60.7	100.8	133.7	92.5
circ segment	LS	2.8	4.0	4.8	5.5	6.1	6.6	7.1	7.6
	AFP	5.0	14.1	22.7	25.3	38.4	50.3	64.2	74.2
	DLP	5.0	13.4	21.2	35.7	67.0	110.0	128.9	147.1
symm lens	LS	2.8	3.8	4.7	5.5	6.0	6.5	7.0	7.4
	AFP	4.8	8.9	21.6	30.6	47.2	45.9	59.2	74.1
	DLP	6.6	9.3	28.3	40.9	62.3	60.7	107.3	194.5
butterfly	LS	2.2	3.4	4.2	5.1	5.6	6.3	6.7	7.2
	AFP	4.3	7.7	14.8	18.1	36.9	40.2	55.7	62.5
	DLP	3.5	13.8	18.8	24.9	48.4	134.6	102.5	103.9

Table 3: Lebesgue constants of least-squares and interpolation on a symmetric sector for different values of ω .

degree		3	6	9	12	15	18	21	24
$\omega = \pi/6$	LS	2.6	3.7	4.7	5.4	6.1	6.7	7.2	7.7
	AFP	3.0	7.8	14.8	23.8	29.1	45.9	54.0	61.6
	DLP	3.0	10.7	18.0	51.3	39.3	104.3	102.4	129.8
$\omega = \pi/2$	LS	2.7	3.7	4.5	5.2	5.7	6.3	6.7	7.2
	AFP	4.8	10.6	16.3	30.5	40.7	46.1	60.0	73.7
	DLP	5.7	16.0	22.0	34.6	61.0	82.2	125.6	125.2
$\omega = 2\pi/3$	LS	2.6	3.9	4.8	5.5	6.1	6.7	7.2	7.3
	AFP	3.3	6.3	17.1	23.7	32.4	42.8	57.4	72.2
	DLP	4.5	9.4	25.7	38.8	96.2	54.1	89.5	131.6

Table 4: Lebesgue constants of least-squares and interpolation on a disk as extremal case of different transformations (cf. Section 2.1.6 and Figures 6-7).

degree		3	6	9	12	15	18	21	24
disk as	LS	3.0	3.9	4.7	5.3	5.9	6.4	7.0	7.4
	symm sector	AFP	3.4	7.3	14.5	28.0	30.7	50.7	68.8
	DLP	4.8	9.1	14.3	38.1	42.8	63.5	110.2	177.5
disk as	LS	2.9	4.0	4.7	5.5	6.3	6.9	7.5	8.0
	asymm sector	AFP	3.7	8.2	13.2	21.1	38.7	47.3	57.8
	DLP	3.7	11.8	24.1	35.5	59.8	79.4	103.5	133.2
disk as	LS	2.7	3.7	4.7	5.3	6.0	6.5	7.1	7.5
	circ zone	AFP	4.5	10.8	14.2	29.6	30.2	62.7	68.8
	DLP	5.5	11.1	25.9	31.8	64.1	60.6	120.6	143.2
disk as	LS	2.7	3.9	4.7	5.4	6.1	6.5	7.0	7.5
	circ segment	AFP	4.1	10.5	19.3	20.5	33.1	54.1	54.1
	DLP	4.1	11.1	19.4	45.4	41.3	69.3	92.2	218.8
disk as	LS	2.1	3.1	3.8	4.6	5.1	5.6	6.0	6.5
	butterfly	AFP	2.7	6.0	9.4	14.9	32.9	31.4	50.5
	DLP	5.6	9.2	18.2	26.9	52.2	71.2	83.5	131.6

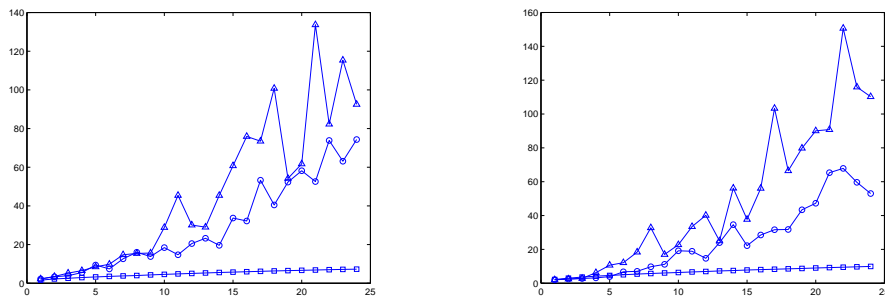


Figure 10: Lebesgue constants of interpolation at approximate Fekete points (circles), discrete Leja points (triangles), and of least-squares fitting on a WAM (squares), for the symmetric sector of Table 2 (left) and for the lune of Figure 9 top-right (right), with $n = 1, 2, \dots, 24$.

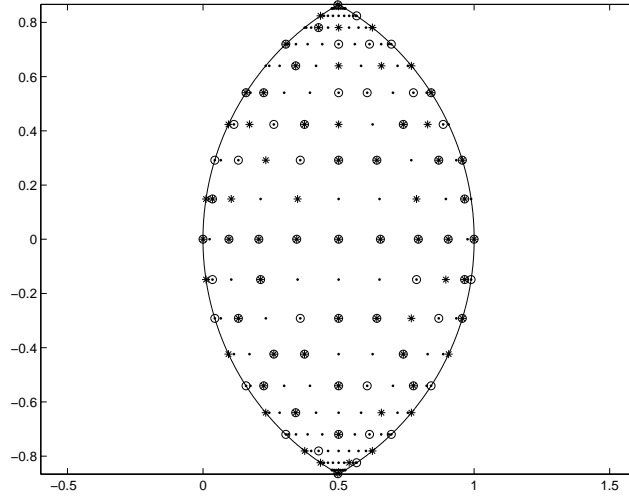


Figure 11: Discrete extremal sets (AFP, circles; DLP, asterisks) extracted from a WAM (dots) for degree 10 on a symmetric lens (top) and on a lune (bottom).

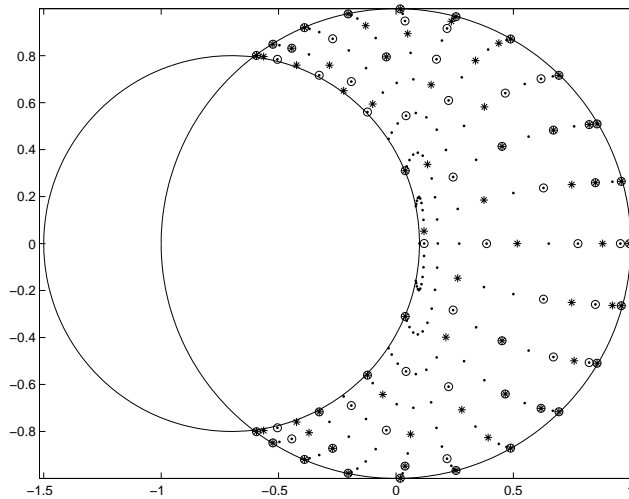


Figure 12: As in Figure 11 for a lune.

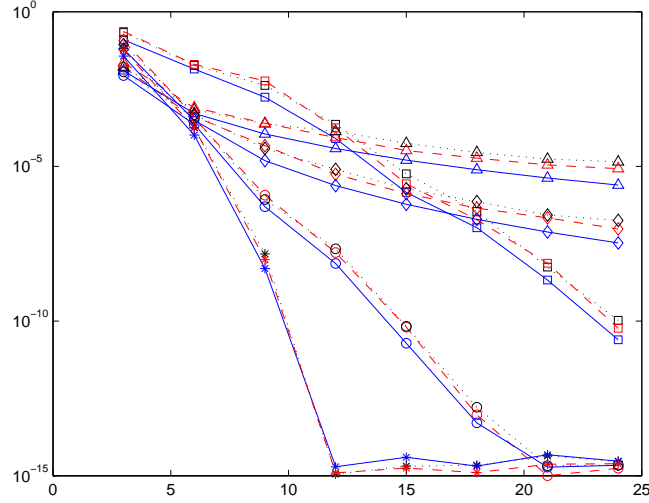


Figure 13: Relative ℓ^2 error of least-squares (solid), interpolation at AFP (dashed) and at DLP (dotted), on the lens of Figure 11 for the test functions f_1 (asterisks), f_2 with $c = 1$ (circles) and $c = 5$ (squares), f_3 with $\delta = 3/2$ (triangles) and $\delta = 5/2$ (diamonds), $n = 3, 6, \dots, 24$, with $(\xi, \eta) = (0.4, 0.4)$.

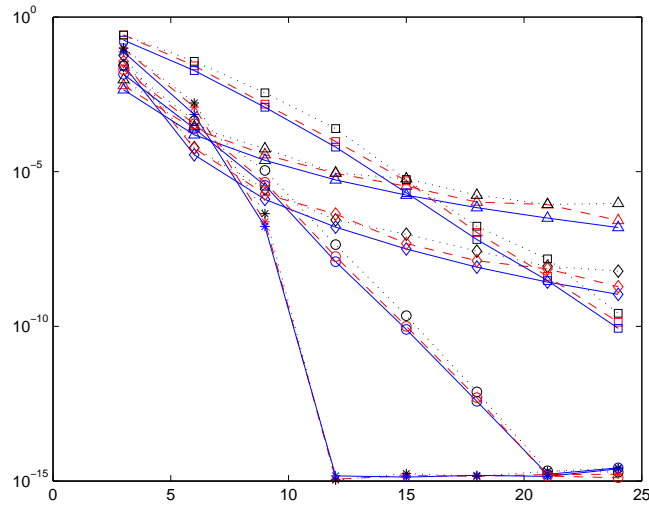


Figure 14: As in Figure 13 for the lune of Figure 12, with $(\xi, \eta) = (0.3, 0.7)$.